Hindawi
Journal of Oncology
Volume 2020, Article ID 4291827, 11 pages
https://doi.org/10.1155/2020/4291827

Research Article

Role of the Exosome Secretion Machinery in Ovarian Carcinoma: *In Vitro* and *In Vivo* Models

Esther Channah Broner,[1] Hadil Onallah,[1] Tali Tavor Re'em,[2] Ben Davidson,[3,4] and Reuven Reich[1]

[1]*Institute of Drug Research, School of Pharmacy, Faculty of Medicine, The Hebrew University of Jerusalem, Jerusalem 91120, Israel*
[2]*Department of Pharmaceutical Engineering, Azrieli College of Engineering, Jerusalem, Israel*
[3]*Department of Pathology, Oslo University Hospital, Norwegian Radium Hospital, Oslo N-0310, Norway*
[4]*University of Oslo, Faculty of Medicine, Institute of Clinical Medicine, Oslo N-0316, Norway*

Correspondence should be addressed to Ben Davidson; bend@medisin.uio.no and Reuven Reich; reuvenr@ekmd.huji.ac.il

Received 6 October 2019; Revised 3 March 2020; Accepted 15 April 2020; Published 30 May 2020

Academic Editor: Vincenzo Coppola

Objective. We recently reported on the expression and clinical role of molecules that mediate exosome secretion in high-grade serous carcinoma. In the present study, the biological role of these molecules was analyzed. *Methods*. OVCAR8 and ES-2 ovarian carcinoma cells were studied using a combination of CRISPR/Cas9 technology and two 3D *in vitro* models—spheroids emulating effusions and alginate scaffolds representing solid lesions. Isolation of exosomes was validated by electron microscopy. *TSAP6*, *NSMASE2*, *RAB27A*, and *RAB27B* mRNA and protein levels were analyzed using qRT-PCR and Western blotting, respectively. Tumor aggressiveness was studied *in vitro* using scratch assay, invasion assay, and matrix metalloproteinase (MMP) activity assay and *in vivo* using a mouse model. *Results*. In OVCAR8 cells, mRNA expression of *TSAP6* and *RAB27A* was significantly higher in spheroids compared to scaffolds, whereas the opposite was true for *NSMASE2* mRNA. In ES-2 cells, *TSAP6* and *RAB27B* mRNA expression was significantly higher in spheroids versus scaffolds. In addition, nSMase2 and TSAP6 protein expression was significantly higher in scaffolds compared to spheroids. CRISPR-edited cells with silencing of *NSMASE2*, *TSAP6*, and *RAB27A/B* had reduced migration, invasion, and MMP activity. Additionally, knockout (KO) of these molecules resulted in significantly diminished exosome secretion. *In vivo* assay showed that when injected to mice, OVCAR8 *RAB27A/B* KO cells, as opposed to control OVCAR8 cells, did not form ascites or visible tumor lesions and had reduced MMP expression. *Conclusion*. The present study provides evidence that different models for culturing ovarian carcinoma cells affect the expression of molecules mediating exosome secretion and that these molecules have a tumor-promoting role. Silencing these molecules may consequently have therapeutic relevance in this cancer.

1. Introduction

Ovarian cancer, the most aggressive gynecologic cancer, was predicted to be diagnosed in 22,530 women and led to 13,980 fatalities in the USA in 2019 [1]. Global figures for 2018 are 295,414 new cases and 184,799 deaths, making this cancer the 8th most common and 8th most lethal cancer in women [2]. While novel targeted therapies, such as PARP inhibitors, have extended the survival of patients carrying mutations in BRCA and related DNA repair genes, prognosis remains dismal for the majority of patients, particularly when the disease is diagnosed at advanced stage [3].

Exosomes are endogenous nanovesicles, 30–120 nm in diameter, that are secreted from cells and are found in bodily fluids including plasma [4], urine [5], saliva [6], breast milk [7], semen [8], and effusions [9, 10]. These nanovesicles contain bioactive molecules including lipids, proteins, DNA, mRNA, miRs, and long noncoding RNA [11, 12].

Exosomes derived from tumor cells have been shown to have cancer-promoting effects, including increased motility

through extracellular matrix (ECM) [13], increased degradation of ECM [14], and invasiveness [15]. Cancer-derived exosomes can also coerce surrounding cells to contribute to their cancer microenvironment: tumor exosomes can transform surrounding fibroblasts into cancer-associated fibroblasts. Exosomes can also cause increased vascular permeability [16], contributing to the metastatic capability of the tumor, as well as condition premetastatic tumor niches at various distant anatomic sites [17, 18].

A previous study by our group reported on anatomic site-dependent expression of components of exosomes secretion machinery, i.e. neutral sphingomyelinase2 (nSMase2), Tumor suppressor-activated pathway 6 (TSAP6), Ras-related protein 27A/B (Rab27a/b) and ADP-ribosylation factor 6 (ARF6) in high-grade serous carcinoma (HGSC), the most common and clinically aggressive histologic type of ovarian carcinoma (OC). TSAP6 and RAB27a levels in effusion specimens were additionally significantly related to overall survival [19].

Another previous study by our group, focusing on Ezrin expression in OC, suggested that tumor growth in a spheroid model closely resembles tumor growth in ascites and pleural effusion, whereas cells cultured on macroporous scaffold are a model for solid tumor growth, thereby creating an inclusive three-dimensional (3D) *in vitro* model that emulates the different anatomic sites affected by OC [20]. In the present study, we utilized this model together with CRISPR-Cas9 Knockouts (KO) in OC cell lines. Our objective was to demonstrate that NSMASE2, TSAP6, and RAB27A/B-related pathways are essential for exosome secretion in OC cell lines and may consequently constitute a potential therapeutic target in OC.

2. Methods and Materials

2.1. Cell Culture. The OVCAR8 and ES-2 OC cell lines were purchased from ATCC (Manassas VA) and cultured at 37°C, 5% CO_2 in their appropriate medium (RPMI + 5% FCS and DMEM + 10% FCS, resp.), supplemented with 1% nonessential amino acids, 1% L-glutamine, 1% BME vitamins, 1% sodium pyruvate and 1% penicillin, streptomycin, and amphotericin. All reagents were purchased from Biological Industries (Beit HaEmek, Israel). OVCAR8 and ES-2 OC spheroids were formed by constant shaking of 400,000 cells per well in 6-well plates for 48 hours on a vertical shaker. Alginate scaffolds with a diameter of 5 mm and thickness of 2 mm were prepared as high guluronic acid (LVG) alginate (NovaMatrix FMC Biopolymers, Drammen, Norway). The macroporous structure was obtained by employing a freeze-drying technique: alginate was dissolved in DDW (1.2% *w*/*v* solution), homogenized and cross-linked with a solution of calcium gluconate (1.2% *w*/*v*) by homogenizer apparatus. The final concentration of cross-linked solution was 1.0% and 0.2% *w*/*v* for the polymer and cross-linker, respectively. The cross-linked solution was doled out into 96-well plates (100 μL/well) and then transferred to +4°C for 1 hour, subsequently to −20°C for 24 hours, and then lyophilized. 400,000 cells were seeded on each alginate scaffold and were cultured for 1-2 weeks.

2.2. Exosome Extraction and Quantitation. 4×10^6 cells were seeded in 100 mm dishes and incubated overnight with supplemented medium of RPMI 5% FCS. On the next day, the medium was replaced with serum-free medium (EXCELL advanced CHO; Sigma-Aldrich, St. Louis MO) and cells were incubated for further 48 hours. The medium was collected and filtered with Amicon Ultra-15 Centrifugal 0.1 μM PVDF Filter Units (Merck Millipore Ltd). Next, the medium was concentrated with 3000 MWCO vivaspin 20 (Sartorius, Göttingen, Germany). Exosomes were extracted from the supernatant according to the user's manual of ExoQuick-TC (System Biosciences, Mountain View CA). The resulting pellet containing exosomes was resuspended in 100 μl of PBS and quantified for protein concentration by Bradford assay. Exosomes were detected and quantified using the qNano Gold analyzer (IZON Science Ltd., Christchurch, New Zealand).

2.3. Electron Microscopy (EM). Exosomes extracted from all genotypes examined were negatively stained with Sodium phosphotungstate (PTA) and imaged by a transmission electron microscope, JEM-1400 plus, available in the Inter-Departmental Equipment Department at the Ein Karem campus of the Hebrew University. This procedure was performed by the staff of the department according to standard protocol. OVCAR8 control-derived exosomes were diluted 1 : 1000 in PBS.

2.4. qRT-PCR. RNA was extracted with Tri-Reagent (Sigma-Aldrich) and converted to cDNA with qScript cDNA synthesis kit (Quanta Biosciences, Gaithersburg MD). qPCR was performed with KAPA SYBERFAST Universal qPCR kit (Kapa Biosystems, Wilmington MA) on the CFX Connect Real-Time system (Bio-Rad Laboratories, Hercules CA). The final concentrations of template and primers were determined individually for every assay, calibrated based on a standard curve. Specific primer sequences were designed utilizing the NCBI Primer Blast tool (Table 1). Analysis was performed with BioRad CFX Manager Software. The ΔCT of genes of interest was calculated relative to the *RPLP0* housekeeping gene and expressed as $2^{-\Delta\Delta CT}$ versus average primary as a control, except for *TSAP6* which was analyzed as *TSAP6/RPLP0*.

When necessary, standard PCR was run using the above equipment and primers with 2G FAST KAPA master mix (Kapa Biosystems). The products were run with electrophoresis on 1.5% agarose gel stained with ethidium bromide, imaged, and then analyzed by ImageJ.

2.5. Immunoblotting. Samples were lysed with 1% NP-40, 20 mM Tris-HCl (pH 7.5), 137 mM NaCl, 0.5 mM EDTA, 10% glycerol, 1% protease inhibitor cocktail (Sigma-Aldrich), and 0.1% SDS and quantified using the Bradford assay. Twenty-five micrograms of protein was loaded on 10% SDS polyacrylamide gels, separated by electrophoresis, and transferred to PVDF membranes (Millipore, Billerica MA) and blocked with 5% nonfat milk in TBST. Primary

Table 1: qPCR primers.

NSMASE2	Forward	5′-AGGACTGGCTGGCTGATTTC-3′
	Reverse	5′-TGTCGTCAGAGGAGCAGTTATC-3′
TSAP6	Forward	5′-GGGAGTTCAGCTTCGTTCAG-3′
	Reverse	5′-TGGGAGGCAGGTAGAACTTG-3′
RAB27A	Forward	5′-GCTTTGGGAGACTCTGGTGTA-3′
	Reverse	5′-TCAATGCCCACTGTTGTGATAA-3′
RAB27B	Forward	5′-TAGACTTTCGGGAAAAACGTGTG-3′
	Reverse	5′-AGAAGCTCTGTTGACTGGTGA -3′

antibodies were as follows: nSMase2 (H00055512-D01; Abnova, Taipei City, Taiwan), TSAP6 (sc-20531; Santa Cruz Biotechnology, Santa Cruz CA), Rab27A (ab55667, Abcam, Cambridge, UK), and GAPDH (14C10, Cell Signaling, Danvers MA). Band density was measured using the Image J software, divided by the loading control (GAPDH), and compared to control.

2.6. CRISPR-Cas9 Knockouts (KO). Clustered Regularly Interspaced Short Palindromic Repeats- (CRISPR-) associated 9 (Cas-9) KOs were generated in OVCAR8 cells using the pSpCas9 (BB)-2A-Puro (PX459) plasmid obtained from Addgene (Watertown MA) according to the manufacturer's protocol. Briefly, specific single guide RNA (sgRNA) inserts were designed to target the beginning of the 5′ sequence of every gene (Table 2).

The inserts were 5′ phosphorylated and annealed on a ramp between 95°C and 25°C. The vector was digested by the BBSI restriction enzyme. Ligation of the insert to the plasmid was performed with T4 ligase. The plasmids were then transformed to DHα5 *E. coli* cells. Plasmids were extracted from the DHα5 *E. coli* cells with GeneJet Plasmid Miniprep (Fermentas Life Sciences) and were sent to the Center for Genomic Technologies at the Hebrew University, Givat Ram, Jerusalem, for sequencing, in order to confirm the insertion of the sgRNA insert. Plasmids were subsequently transfected into OVCAR8 cells with Lipofectamine 2000 (Invitrogen, Carlsbad CA). Selection by Puromycin (A.G. Scientific Inc. San Diego CA) was performed, and the surviving resistant cells were seeded as single cell colonies, resulting in formation of single cell clones of-KO cells, which were then analyzed for KO with PCR or qPCR as described above.

2.7. Migration—Scratch Assay. OVCAR8 cells with *NSMASE, TSAP6,* and *RAB27A/B* KOs and OVCAR8 control cells were seeded to confluence in 6-well plates. Each well was scratched twice with a sterile tip. The scratch in *NSMASE2* and *TSAP6* KO cells was imaged at $t = 0$ and $t = 18$ hrs. *RAB27A/B* KOs were imaged at $t = 0$ and $t = 24$ hrs. Wound closure was analyzed by T-scratch software [21].

2.8. Matrix Metalloproteinases (MMP) Activity Assay. KO cells and OVCAR8 control cells ($n = 500{,}000$) were incubated overnight in DMEM medium supplemented with 0.1% BSA. The conditioned medium was loaded on 1 mg gelatin/ml, 10% SDS polyacrylamide gels, and separated by electrophoresis. The gels were incubated overnight at 37°C and then washed in 2.5% triton, developed, dried, and analyzed with the ImageJ software.

2.9. Invasion Assay. Cells of all genotypes ($n = 50{,}000$) were seeded on Matrigel-coated filters in Boyden chambers and incubated for 6 hours at 37°C with conditioned medium from the 3T3 fibroblast cell line, used as chemoattractant. Invading cells were stained and quantified under an invert microscope.

2.10. In Vivo Tumor Aggressiveness Assay. OVCAR8, RAB27A-KO, and RAB27B-KO cells (2×10^6) were injected IP into female SCID mice ($n = 12$; 5 controls, 4 *RAB27A*-KO, 3 *RAB27B*-KO). Mice were monitored for 21 days, until symptoms of OC appeared. The tumors were removed, fixed in formalin, and embedded in paraffin. H&E sections were assessed by an experienced surgical pathologist (BD). The presence of ascites fluid was noted. All experiments were authorized by the Animal Ethics Committee of the Hebrew University of Jerusalem.

2.11. Immunohistochemistry (IHC). Formalin-fixed, paraffin-embedded sections from the *in vivo* mouse model were analyzed for Ki-67, p53, MMP2, and MMP9 protein expression using the Dako EnVision System (Dako, Glostrup, Denmark). The Ki-67 antibody was a rabbit polyclonal antibody purchased from Abcam (cat no. 15580; Cambridge, UK), applied at 1 : 1000 dilution with antigen retrieval in HpH (pH 9.0) solution (Dako). The p53 antibody was a rabbit polyclonal antibody purchased from Novocastra (part of Leica Biosystems; cat no. NCL-p53-CM1; Wetzlar, Germany), applied at 1 : 3000 dilution with antigen retrieval in citrate buffer (pH 6.0). The MMP2 antibody was a rabbit polyclonal antibody purchased from LabVision (cat no. RB-9233-P1; Fremont CA), applied at 1 : 400 dilution with antigen retrieval in Tris-EDTA buffer. The MMP9 antibody was a rabbit polyclonal antibody purchased from NeoMarkers (part of LabVision; cat no. RB-1539-P1; Fremont CA), applied at 1 : 200 dilution with no antigen retrieval. Positive controls consisted of normal spleen (Ki-67), colon carcinoma (p53), placenta (MMP2), and lung carcinoma (MMP9).

2.11.1. IHC Scoring. Nuclear staining was scored as positive for Ki-67 and p53 and cytoplasmic staining for MMP2 and MMP9. Scoring was performed by an experienced surgical pathologist (BD), using a 0–4 scale as follows: 0 = no staining, 1 = 1–5%, 2 = 6–25%, 3 = 26–75%, 4 = 76–100% of tumor cells.

2.12. Statistical Analysis. Student's t-test was employed, significance was determined as $p < 0.05$. High and low mRNA and protein expression was defined relative to expression in control cells in each experiment.

Table 2: CRISPR-Cas9 sgRNA insert sequences.

NSMASE2	Sense	CACCGTTCACCTCGGTGGGCCATG
	Antisense	AAACCATGGCCCACCGAGGTGAAC
TSAP6	Sense	CACCGCCATTGCAAACTCGCTCAAC
	Antisense	AAACCGTTGAGCGAGTTTGCAATGG
RAB27A	Sense	CACCCAGTATTCATACCCACTCCG
	Antisense	AAACCGGAGTGGGTATGAATACTG
RAB27B	Sense	CACCGCACTCGCAGTCCTGACGGGGCAGGG
	Antisense	AAACCCCCTGCCCGTCAGGACTGCGAGTG

3. Results

3.1. Growth Form in 3D Models Influences Gene and Protein Expression in OC. Our aim was to develop a 3D model that emulates OC. To this end, we successfully introduced two separate 3D *in vitro* models utilizing the OVCAR8 and ES-2 OC cell lines—a spheroid model and a scaffold model.

Analysis of the genes involved in exosome secretion in OVCAR8 cells showed different *NSMASE2, TSAP6*, and *RAB27A* levels as function of the culture method (Figures 1(a)–1(d)). mRNA expression of *TSAP6* and *RAB27A* was higher in spheroids compared to scaffolds ($p < 0.01$ and $p < 0.001$, respectively), whereas the opposite was true for *NSMASE2* mRNA ($p = 0.0001$). No change was observed in *RAB27B* mRNA levels. In ES-2 cells, *TSAP6* and *RAB27B* mRNA expression was higher in spheroids versus scaffolds ($p < 0.03$, $p < 0.02$, respectively) (Supplementary Figures 1(a) and 1(b)).

nSMase2 and TSAP6 protein expression was higher in scaffolds compared to spheroids ($p < 0.006$ and $p < 0.0004$, respectively). The growth form did not affect RAB27A protein expression (Figures 2(a)–2(c), Supplementary Figure S2). RAB27B protein expression was not analyzed due to lack of adequate antibody.

3.2. CRISPR Cas9 KO in OC Cell Lines. In order to evaluate the distinct role of the genes putatively involved in exosome secretion, OVCAR8 cells were subjected to KO with the CRISPR Cas9 protocol for the various genes in this study. KOs were validated by qPCR showing the absence of mRNA and by Western Blot, proving that this gene was silenced and not expressed in this cell line. The percentages of KO achieved and protein levels are detailed in Table 3.

3.3. Exosome Secretion Pathway KO Leads to Decreased Exosome Secretion in OC Cell Lines. EM visualization showed that under normal culture conditions, OVCAR8 cells secrete exosomes (Figure 3(a)). However, when measured by the qNano Gold analyzer, exosome secretion was significantly reduced in OVCAR8 KO cells compared to control OVCAR8 cells (*TSAP6 KO*: $p < 0.05$; *RAB27A KO*: $p < 0.05$; *RAB27B KO*: $p < 0.01$; Figure 3(b)).

3.4. Suppression of Exosome Secretion Pathways Leads to Reduced Migration, MMP Activity, and Invasion in OC Cells. OVCAR8 cells with KO of any of the four genes, that is, *NSMASE2*, *TSAP6*, *RAB27A*, and *RAB27B*, migrated significantly less in the scratch assay (Figure 4(a)). After 24 hours, the wounds in OVCAR8 cells with KO mutation of *NSMASE2* and *TSAP6* were 73% and 55% open, respectively, versus 27% of the OVCAR8 control ($p < 0.001$ and $p < 0.03$, resp.).

RAB27A/B KO wounds analyzed after 18 hours were 81% and 71% open versus 43% of the control ($p < 0.0001$ and $p < 0.0005$, respectively).

In MMP activity tests, MMP9 activity was significantly reduced in OVCAR8 *NSMASE2*, *TSAP6*, and *RAB27A* KO cells compared to OVCAR8 control cells ($p < 0.05$; Figure 4(b)).

In the Boyden chamber invasion assay, OVCAR8 *RAB27A/B* KO cells infiltrated significantly less than control OVCAR8 cells: an average of 32 and 44 cells succeeded in infiltrating, respectively, versus an average of 73 cells in the control ($p < 0.0005$ and $p < 0.05$, respectively). A trend was noted for *NSMASE2*-KO cells where only 52 cells infiltrated ($p = 0.087$; Figure 4(c)).

3.5. Suppression of Exosome Secretion Pathways Leads to Absence of Ascites Fluid and Reduced Tumor Size In Vivo. Seven weeks following the injection of 2×10^6 cells of OVCAR8 control, *RAB27A*-KO and *RAB27B*-KO to SCID mice, only the mice injected with OVCAR8 control cells developed ascites, with a volume ranging from 0.75 to 1.5 ml. No ascites ascites was observed in the mice injected with KOs. The entire group of *RAB27A*-KO and *RAB27B*-KO mice exhibited no visible tumors by gross examination, whereas tumor nodules were detected in the OVCAR8 control group. Microscopic assessment of the abdominal organs from the 12 mice showed that in *RAB27A*-KO and *RAB27B*-KO mice, the majority of organs were tumor-free, with isolated tumor nodules ranging from 0.5 mm to 4 mm and 0.5 to 2 mm, respectively, whereas the OVCAR8 control group had multiple lesions with a diameter of up to 7 mm (Figure 5, Supplementary Table S1). The average diameter of metastasis, including tumor-negative organs, was 0.59 mm for the *RAB27A*-KO group (total diameter of all metastases 13.5 mm in 23 organs), 0.35 mm for the *RAB27B*-KO group (total diameter of all metastases 5.5 mm in 16 organs), and 1.53 mm for the control group (total diameter of all metastases 44.5 mm in 29 organs; $p < 0.05$).

IHC analysis showed comparable expression of Ki-67 and p53 in tumors from the *RAB27A*-KO and *RAB27B*-KO mice compared to controls. However, MMP2 and MMP9 expression

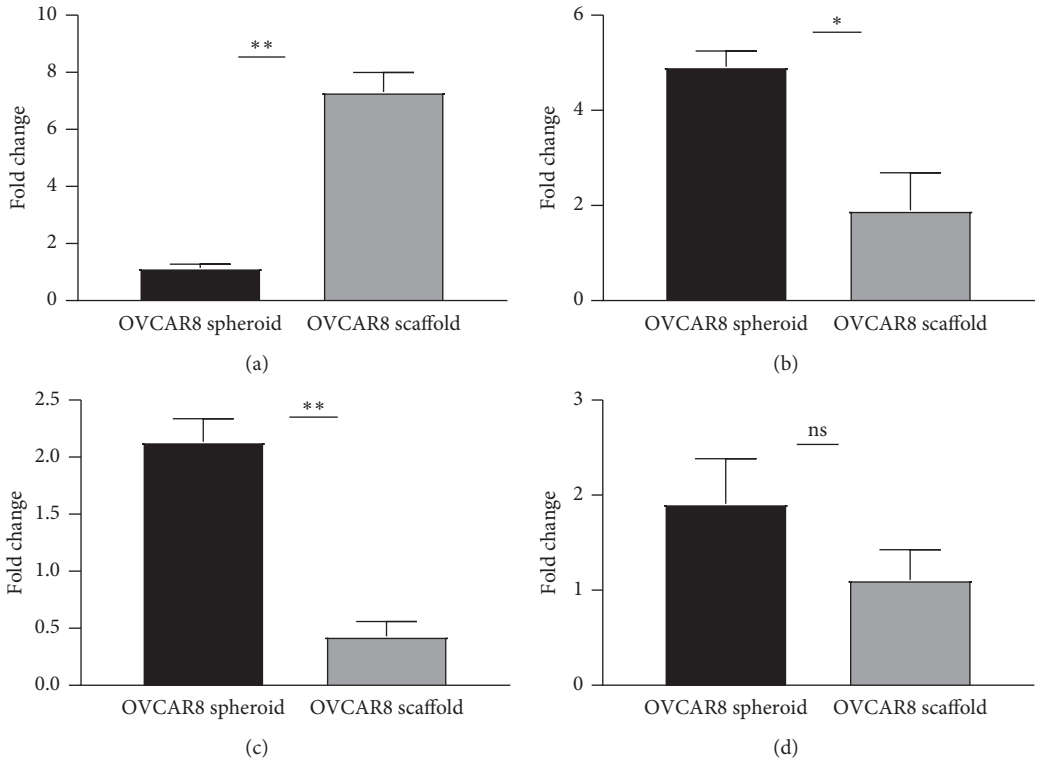

Figure 1: (a–d) Gene expression dependent on 3D cell culture form: differential expression of mRNA expression in spheroids and scaffolds is seen for the following genes: (a) *NSMASE2* ($p = 0.0001$), (b) *TSAP6* ($p < 0.01$), (c) *RAB27A* ($p < 0.001$), (d) *RAB27B* ($p < 0.55$) in OVCAR8 cells.

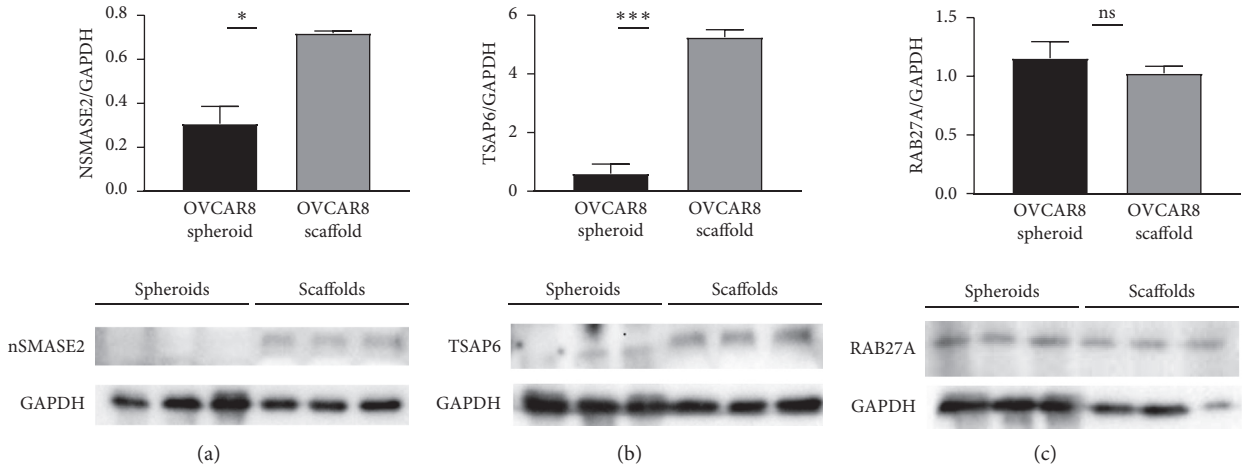

Figure 2: (a–c) Differential protein expression depending on 3D growth form in OVCAR8 cell line: (a) nSMase2 and (b) TSAP6 protein expression is higher in scaffolds compared to spheroids ($p < 0.006$ and $p < 0.0004$, respectively). (c) RAB27A protein expression is not affected by growth form; error bars indicate SEM.

was significantly lower in tumors from *RAB27A*-KO and *RAB27B*-KO mice (Figure 6; Supplementary Table S1).

4. Discussion

We previously reported on the frequent expression and clinical relevance of several molecules belonging to the exosome secretion machinery in HGSC cells and tumor-derived exosomes [19]. In the present study, we analyzed whether a novel 3D OC model representing OC progression can be relevant for studying exosome secretion pathways in this cancer.

We propose that alginate scaffolds emulate solid tumors, while spheroids mimic tumor growth in effusions. In the

Table 3: Percentage of KO generated by CRISPR Cas9 in OVCAR8 cells.

	KO
A. qPCR	
NSMASE2	90%
TSAP6	90%
RAB27A	85%
RAB27B	99%
B. Western blot	

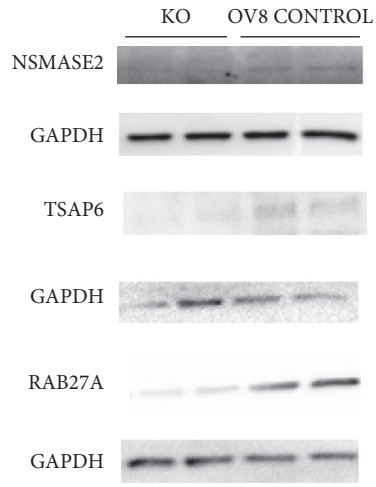

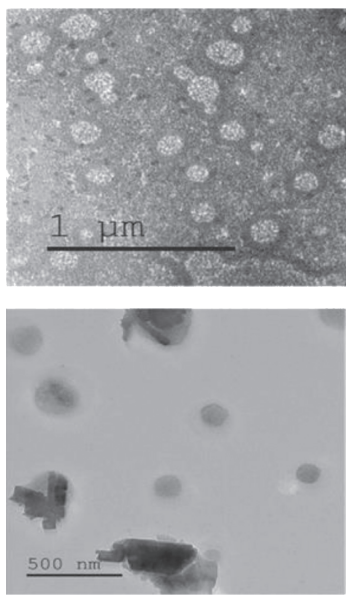

OVACAR8-derived exosomes

(a)

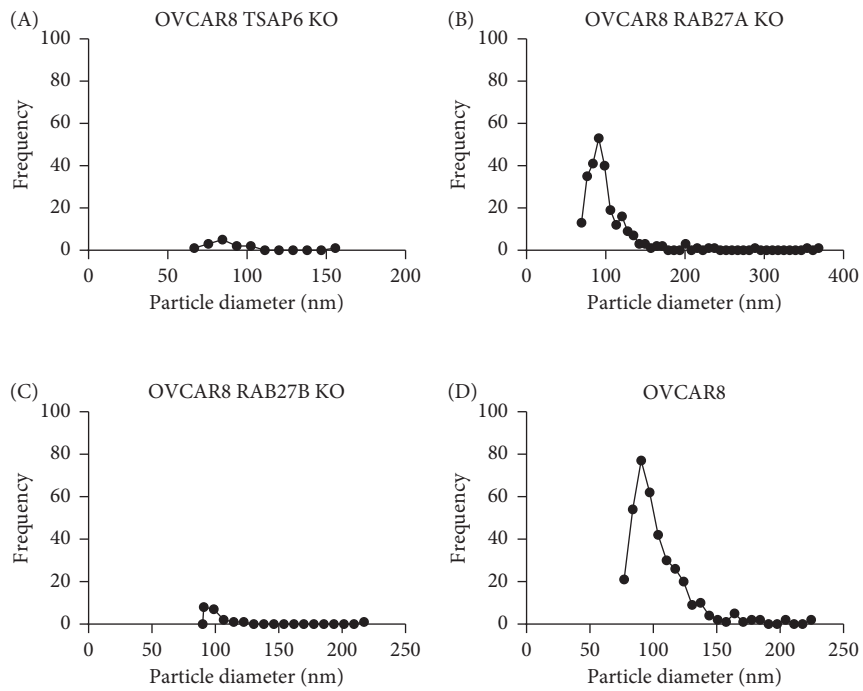

(b)

Figure 3: (a) OVCAR8-derived exosomes, diameter 40–120 nm, as visualized by EM; PTA staining, X10K magnification (top), and X5K magnification (bottom). Scale bar indicates the size of the field shown. (b) Exosome secretion in OVCAR8 KO cell lines: exosome secretion is reduced in (A) TSAP6 KO, (B) RAB27A KO, and (C) RAB27B KO compared to (D) OVCAR8 control cell lines.

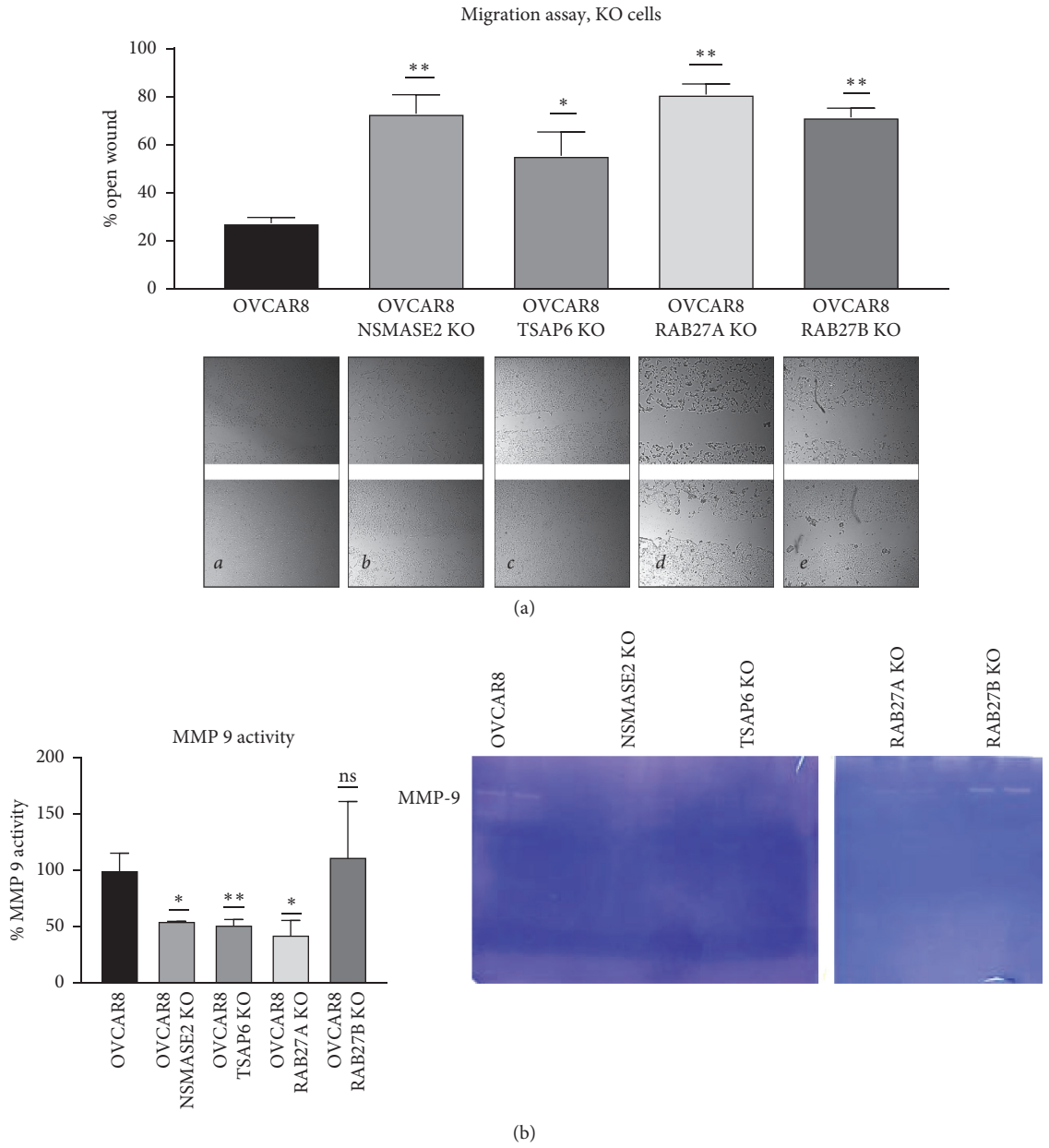

Figure 4: Continued.

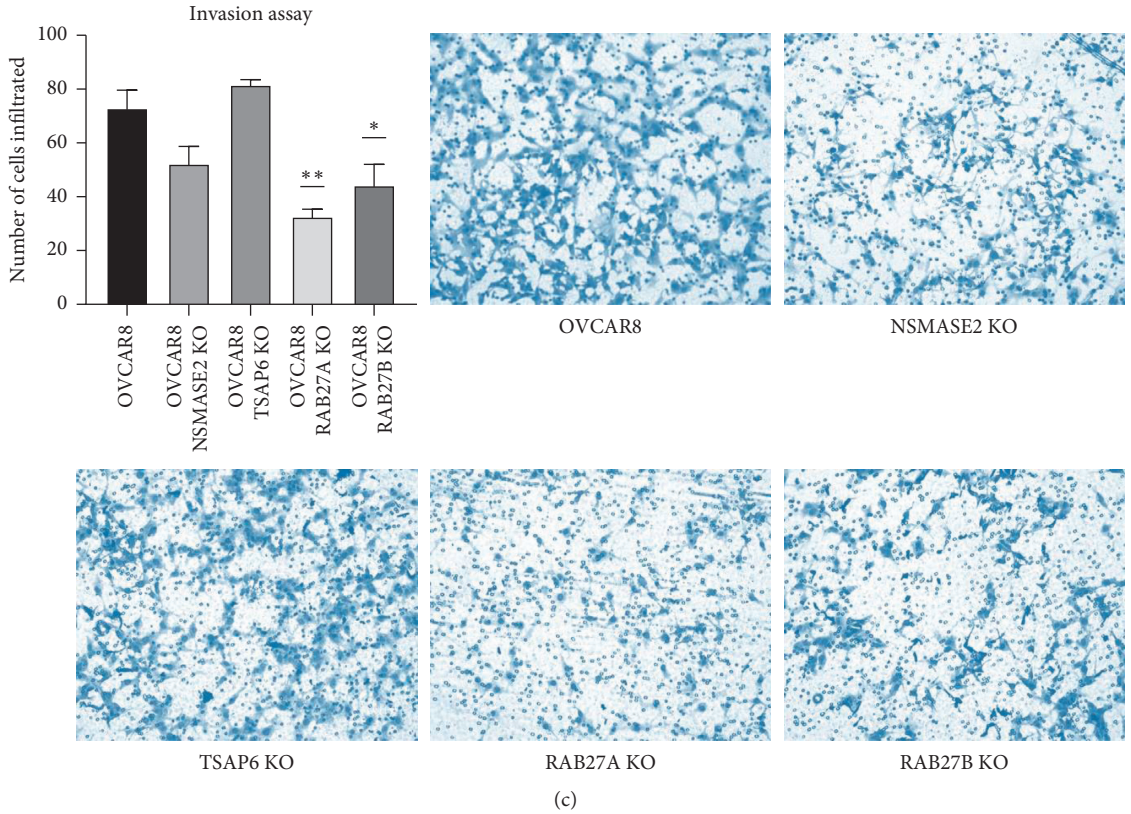

Figure 4: (a) Migration assay. Below: extent of the wound open after 18 or 24 hours, respectively: (a) OVCAR8 control, (b) *NSMASE2*-KO ($p < 0.001$, $n = 4$), (c) *TSAP6*-KO ($p < 0.03$, $n = 4$), (d) *RAB27A*-KO ($p < 0.0001$, $n = 8$), (e) *RAB27B*-KO ($p < 0.001$, $n = 8$). Above: quantification of experiment. Error bars represent SEM. (b) MMP activity assay. The width of the MMP9 gelatin consumed band is reduced in OVCAR8 *NSMASE2* ($p < 0.05$), *TSAP6* ($p < 0.01$), and *RAB27A* ($p < 0.03$) KO cells, but not in *RAB27B* KO cells. Error bars represent SEM. (c) Invasion assay: cells infiltrating through matrigel filters were quantified in this assay. *RAB27A/B-KO* cells infiltrated less than the OVCAR8 control cells. $p < 0.0005$ and $p < 0.05$, respectively. Error bars represent SEM.

present study we show that the 3D form of growth influences both the mRNA and protein expression of the exosome secretion pathway in OC cell lines, as reflected by changes in *NSMASE2*, *TSAP6*, *RAB27A*, and *RAB27B* mRNA, as well as NSMASE2 and TSAP6 protein expression depending on the 3D form applied.

In OVCAR8 cells, *TSAP6* and *RAB27A* mRNA levels were higher in spheroids than in scaffolds and *RAB27B* mRNA expression was not influenced by the growth form. This profile partly concurs with our findings in our previous study [19], where *TSAP6* mRNA expression levels were higher in HGSC effusions compared to surgical specimens, while those of *RAB27B* expression did not differ between these anatomic locations. Data are discordant with respect to *RAB27A* mRNA, which had comparable expression levels in solid lesions and effusions, despite the use of the same assay, presumably due to inherent differences between cell lines and clinical specimens. NSMASE2 and TSAP6 protein levels were higher in scaffolds compared to spheroids, in agreement with the higher NSAMSE2 and TSAP6 expression in solid tumors versus effusions in our previous study. These data suggest that the different culture models faithfully emulate 3D growth in solid lesions and effusions in HGSC.

Of note, there were notable differences between the mRNA and protein expression levels of Rab27A and TSAP6. We hypothesize this discrepancy to result from the action of molecules regulating mRNA levels or due to epigenetic regulation of protein expression.

We utilized the CRISPR-Cas9 system and produced *NSMASE2*, *TSAP6*, *RAB27A*, and *RAB27B* KOs in the OVCAR8 cell line. EM showed that OVCAR8 cells produce exosomes. The secretion of these exosomes was significantly diminished in *RAB27A*-KO, *RAB27B*-KO, and *TSAP6*-KO cells, well in agreement with the study of Bobrie et al., in which Rab27a mediated exosome secretion in breast carcinoma cells [22]. Of note, in another study by the same group, Rab27a silencing reduced docking of multivesicular endosomes (MVEs) and increased their size in Hela cells, whereas MVEs were redistributed towards the perinuclear region upon Rab27b silencing, documenting that these two proteins have different roles [23].

Functional assays in the present study showed that molecules involved in the exosome machinery also regulate critical cancer-related processes. In migration assays, all KO cells migrated significantly less, indicating that these genes, perhaps via exosome secretion, are needed for this metastatic feature. In the zymography assay that assesses the ability of

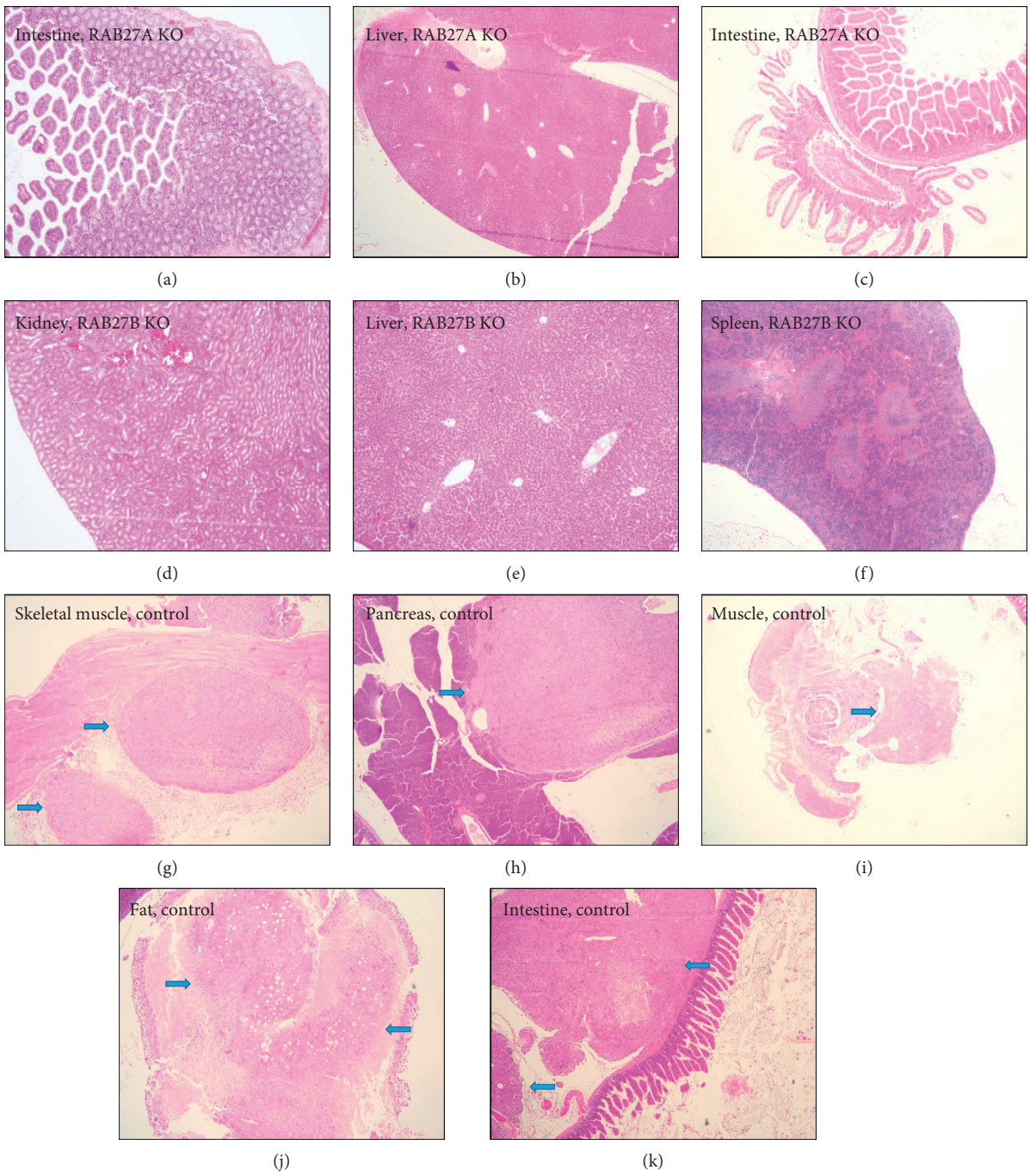

FIGURE 5: Six sections from the liver, kidney, spleen, and intestine of mice in the *RAB27A*-KO and *RAB27B*-KO groups. No tumor nodules are seen. (g–k) Five sections of tumor nodules (marked with blue arrows) in the pancreas, intestine, muscle, and fat tissue in the OVACR control group (all figures at ×100 magnification). Differences in average tumor diameter between the KO groups and controls were significant ($p < 0.05$; see text).

cancer cells to degrade gelatin via MMPs, *NSMASE2*-KO, RAB27A-KO, and *TSAP6*-KO cells showed reduced MMP9 activity. In the Boyden Chamber invasion assay that measures another metastatic characteristic, that is, the ability to degrade matrigel, *RAB27A*-KO and *RAB27B*- KO cells infiltrated significantly less. This finding is well in agreement with the study of Gebäck et al. [21], in which Rab27A silencing resulted in decreased MMP9 activity, suppressed growth of the primary tumor, and reduced lung dissemination following the injection of 4T1 metastatic carcinoma cells to mice. Overall, exosome pathway KO cells appear to possess less malignant and less metastatic characteristics, suggesting that the exosome machinery pathway is important for tumor progression.

The development of a malignant effusion in the peritoneal and/or pleural cavities represents metastatic disease

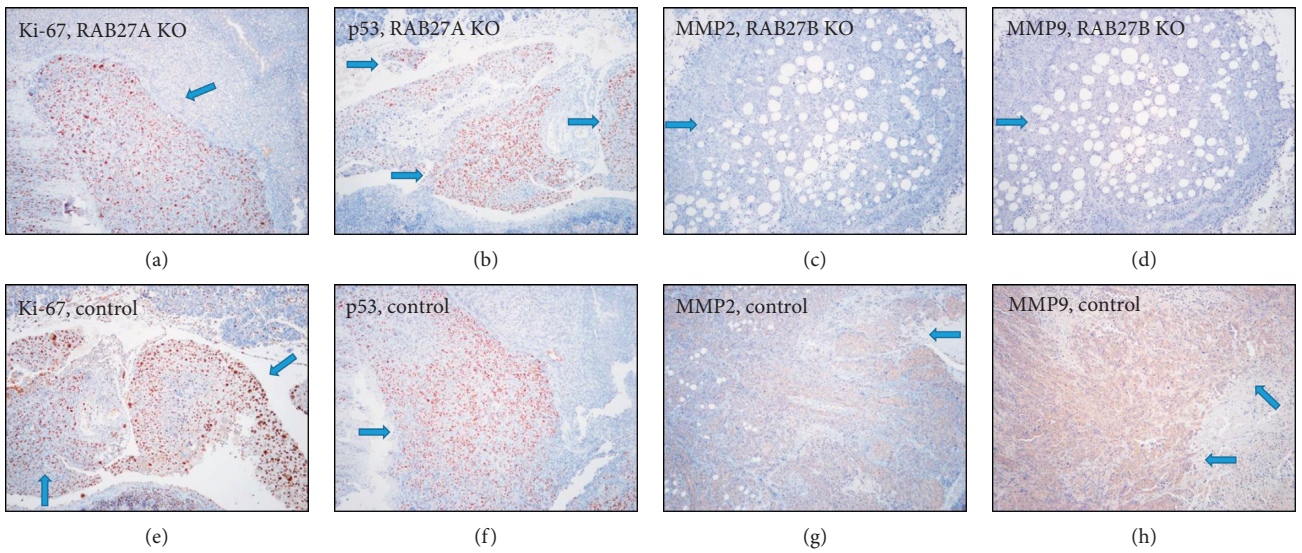

Figure 6: Protein expression of Ki-67, p53, MMP2, and MMP9 by IHC. Ki-67 and p53 expression is comparable in *RAB27A*-KO cells and controls. In contrast, a *RAB27B*-KO shows no expression of MMP2 and MMP9, whereas control cells are diffusely positive for both proteins. Tumor areas are marked with blue arrows (all figures at ×100 magnification).

that is not amenable to surgical removal, where tumor cells are chemoresistant and possess cancer stem cell characteristics [24, 25]. This form of tumor progression is therefore a highly lethal stage of OC, in addition to its detrimental effect on the quality of life of OC patients. In contrast to OVCAR8 controls, no development of ascites was observed following injection of *RAB27A* and *RAB27B* KO cells to mice, and solid tumor nodules were significantly smaller, indicating that these molecules may have direct clinical relevance in HGSC. Tumors from mice injected with *RAB27A* and *RAB27B* KO cells additionally had lower MMP expression. Overall, the experimental data, combined with the association between TSAP and poor outcome in our previous study [19], support a role as oncogenes rather than tumor suppressors for the exosome machinery components. An association between Rab27a protein and favorable outcome was nevertheless observed for exosomal levels of this protein in our previous study [19], raising the possibility that extracellular Rab27a has other functions than its intracellular counterpart.

In conclusion, this study presents a 3D *in vitro* model that may allow exploration of the molecular drivers of the different growth forms of OC. Our *in vivo* model shows that interfering with the exosome secretion pathway contributes to attenuating the aggressiveness of OC, a finding that may have therapeutic relevance. Analysis of the content of exosomes derived from the scaffold and spheroid model, including proteins, mRNA, and noncoding RNA, may be of interest in future research.

Data Availability

The experimental data used to support the findings of this study are included within the article. Additional information regarding this study is available from the corresponding author upon request.

Conflicts of Interest

The authors have no conflicts of interest.

Authors' Contributions

Esther Channah Broner performed the experiments and wrote the manuscript. Hadil Onallah performed the experiments and critically read the manuscript. Tali Tavor Re'em prepared the 3D constructs and critically read the manuscript. Ben Davidson designed the study, microscopically assessed the tumors in the mice experiments, performed and scored the immunostains, and co-wrote the manuscript. Reuven Reich designed the study, supervised the experiments, and cowrote the manuscript. Esther Channah Broner and Hadil Onallah contributed equally to this work.

Supplementary Materials

Figure 1: (a) RAB27B ($p < 0.02$) and (b) TSAP6 ($p < 0.03$) mRNA expression in the ES-2 cell line. Figure 2: images of the actual Western blots of Figures 2(a)–2(c). Table S1: Isolated tumor nodules ranges in mm in the various organs. (*Supplementary Materials*)

References

[1] R. L. Siegel, K. D. Miller, and A. Jemal, "Cancer statistics, 2019," *CA: A Cancer Journal for Clinicians*, vol. 69, no. 1, pp. 7–34, 2019.

[2] F. Bray, J. Ferlay, I. Soerjomataram, R. L. Siegel, L. A. Torre, and A. Jemal, "Global cancer statistics 2018: GLOBOCAN estimates of incidence and mortality worldwide for 36 cancers in 185 countries," *CA: A Cancer Journal for Clinicians*, vol. 68, no. 6, pp. 394–424, 2018.

[3] S. Lheureux, C. Gourley, I. Vergote, and A. M. Oza, "Epithelial ovarian cancer," *The Lancet*, vol. 393, no. 10177, pp. 1240–1253, 2019.

[4] M.-P. Caby, D. Lankar, C. Vincendeau-Scherrer, G. Raposo, and C. Bonnerot, "Exosomal-like vesicles are present in human blood plasma," *International Immunology*, vol. 17, no. 7, pp. 879–887, 2005.

[5] T. Pisitkun, R.-F. Shen, and M. A. Knepper, "Identification and proteomic profiling of exosomes in human urine," *Proceedings of the National Academy of Sciences*, vol. 101, no. 36, pp. 13368–13373, 2004.

[6] M. Gonzalez-Begne, B. Lu, X. Han et al., "Proteomic analysis of human parotid gland exosomes by multidimensional protein identification technology (mudpit)," *Journal of Proteome Research*, vol. 8, no. 3, pp. 1304–1314, 2009.

[7] C. Admyre, S. M. Johansson, K. R. Qazi et al., "Exosomes with immune modulatory features are present in human breast milk," *The Journal of Immunology*, vol. 179, no. 3, pp. 1969–1978, 2007.

[8] A. Poliakov, M. Spilman, T. Dokland, C. L. Amling, and J. A. Mobley, "Structural heterogeneity and protein composition of exosome-like vesicles (prostasomes) in human semen," *The Prostate*, vol. 69, no. 2, pp. 159–167, 2009.

[9] M. P. Bard, J. P. Hegmans, A. Hemmes et al., "Proteomic analysis of exosomes isolated from human malignant pleural effusions," *American Journal of Respiratory Cell and Molecular Biology*, vol. 31, no. 1, pp. 114–121, 2004.

[10] B. P. Foster, T. Balassa, T. D. Benen et al., "Extracellular vesicles in blood, milk and body fluids of the female and male urogenital tract and with special regard to reproduction," *Critical Reviews in Clinical Laboratory Sciences*, vol. 53, no. 6, pp. 379–395, 2016.

[11] B. K. Thakur, H. Zhang, A. Becker et al., "Double-stranded DNA in exosomes: a novel biomarker in cancer detection," *Cell Research*, vol. 24, no. 6, pp. 766–769, 2014.

[12] E. R. Abels and X. O. Breakefield, "Introduction to extracellular vesicles: biogenesis, rna cargo selection, content, release, and uptake," *Cellular and Molecular Neurobiology*, vol. 36, no. 3, pp. 301–312, 2016.

[13] B. H. Sung, T. Ketova, D. Hoshino, A. Zijlstra, and A. M. Weaver, "Directional cell movement through tissues is controlled by exosome secretion," *Nature Communications*, vol. 6, p. 7164, 2015.

[14] S. Yue, W. Mu, U. Erb, and M. Zöller, "The tetraspanins CD151 and tspan8 are essential exosome components for the crosstalk between cancer initiating cells and their surrounding," *Oncotarget*, vol. 6, no. 4, pp. 2366–2384, 2015.

[15] J. W. Clancy, A. Sedgwick, C. Rosse et al., "Regulated delivery of molecular cargo to invasive tumour-derived microvesicles," *Nature Communications*, vol. 6, no. 1, 2015.

[16] H. Peinado, M. Alečković, S. Lavotshkin et al., "Melanoma exosomes educate bone marrow progenitor cells toward a pro-metastatic phenotype through MET," *Nature Medicine*, vol. 18, no. 6, pp. 883–891, 2012.

[17] B. Costa-Silva, N. M. Aiello, A. J. Ocean et al., "Pancreatic cancer exosomes initiate pre-metastatic niche formation in the liver," *Nature Cell Biology*, vol. 17, no. 6, pp. 816–826, 2015.

[18] M. Tkach and C. Théry, "Communication by extracellular vesicles: where we are and where we need to go," *Cell*, vol. 164, no. 6, pp. 1226–1232, 2016.

[19] E. C. Broner, C. G. Tropé, R. Reich, and B. Davidson, "TSAP6 is a novel candidate marker of poor survival in metastatic high-grade serous carcinoma," *Human Pathology*, vol. 60, pp. 180–187, 2017.

[20] V. Horwitz, B. Davidson, D. Stern, C. G. Tropé, T. Tavor Re'em, and R. Reich, "Ezrin is associated with disease progression in ovarian carcinoma," *PLoS One*, vol. 11, Article ID e0162502, 2016.

[21] T. Gebäck, M. M. P. Schulz, P. Koumoutsakos, and M. Detmar, "TScratch: a novel and simple software tool for automated analysis of monolayer wound healing assays," *Biotechniques*, vol. 46, no. 4, pp. 265–274, 2009.

[22] A. Bobrie, S. Krumeich, F. Reyal et al., "Rab27a supports exosome-dependent and -independent mechanisms that modify the tumor microenvironment and can promote tumor progression," *Cancer Research*, vol. 72, no. 19, pp. 4920–4930, 2012.

[23] M. Ostrowski, N. B. Carmo, S. Krumeich et al., "Rab27a and Rab27b control different steps of the exosome secretion pathway," *Nature Cell Biology*, vol. 12, no. 1, pp. 19–30, 2010.

[24] B. Davidson, "Recently identified drug resistance biomarkers in ovarian cancer," *Expert Review of Molecular Diagnostics*, vol. 16, no. 5, pp. 569–578, 2016.

[25] B. Davidson, "Biomarkers of drug resistance in ovarian cancer—an update," *Expert Review of Molecular Diagnostics*, vol. 19, no. 6, pp. 469–476, 2019.